

Chapter 5

VANS macroscopic applications

The first principle is that you must not fool yourself — and you are the easiest person to fool.

- 1974 Caltech commencement address, *Richard Feynman*

5.1 Introduction

In this chapter the macroscopic VANS equation are validated against a full microscopic DNS. Special attention is focused on the interface treatment using the penalization method. We also assess the effects of the permeability tensor metamodel ~~introduction~~ in the algorithm. The computation is performed using the classical closed cavity configuration. The aim for the cavity problem is to validate the VANS approach and show the importance of the interface treatment and the permeability metamodel. In the last part the Ercoftac periodic hill case is also tested. This open configuration aims to test the performance of porous coating as a device ~~to help~~ to reduce separated flow.

5.2 Closed cavity problem

The configuration chosen is the square closed cavity, depicted in figure 5.1. The cavity is square shaped with size L , the lateral and bottom walls are fixed and a constant velocity U_{top} is specified at the top side. On the front and back side we apply periodic boundary conditions since the simulation domain has a depth equal to ℓ . A rigid porous ~~medium~~ made by regularly arranged fibers is set at the bottom of the cavity, its vertical extension is equal to h . The reference elementary volume (REV) of the porous medium is a cubic cell of size ℓ with a cylinder, with diameter d , at ~~its~~ center. The porosity of the medium ε is equal to 0.8 and ~~with~~ 50 fibers in the cavity.

To summarize the configuration:

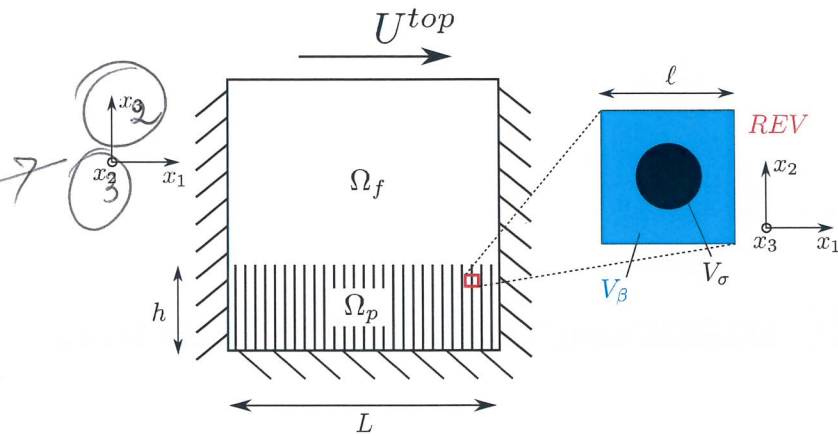


Figure 5.1: Schematics of the closed cavity 2D problem. The porous medium internal structure is depicted in the zoom on the right side in which the REV geometry is shown.

- L : side of the cavity, also the macroscopic length scale
- h : vertical extension of the fibers from the bottom of the cavity
- ℓ : side of the cubic REV, also the microscopic length scale
- d : diameter of the cylindrical fiber
- V_β : volume of the fluid inside the REV
- V_σ : volume of the solid inside the REV
- $\varepsilon = \frac{V_\beta}{V_\sigma + V_\beta}$: porosity of the medium
- $\epsilon = \frac{\ell}{L}$: length scale ratio
- $Re = \frac{U_{top} L}{\nu_\beta}$: Reynolds number of the cavity

$$= \frac{\ell^3 - \ell \pi d^2/4}{\ell^3} = 1 - \pi \left(\frac{d}{2\ell} \right)^2$$

The overall domain has the size $L \times L \times \ell$ respectively in the x_1 , x_2 and x_3 directions. The origin of our coordinate system at the bottom left corner of the cavity. This configuration and porous arrangement has been chosen to reuse DNS data already available for this configuration (private communication with ~~the authors~~ Zampogna and Bottaro [165]).

The length parameters for the specific case are:

- $h/L = 0.33$

- $\ell/L = 0.02$
- $\varepsilon = 0.8$

5.2.1 Microscopic approach with direct numerical simulations

In this approach the incompressible Navier-Stokes equations are solved in the three dimensional case (5.1). The problem is weakly three dimensional ~~problem~~ since we include only one REV in the x_3 axes and we impose periodic boundary condition in this direction. This assumption seems fair since the Reynolds numbers tested are small and no 3D structures are expected in the flow. To complete the set of boundary condition the no-slip condition is applied at the rigid walls and a prescribed horizontal velocity is imposed at the top wall (5.1). The subscript β means that the variables belongs to the fluid phase, as usual. The mesh was fine enough to resolve the flow ~~inside~~ within the fibers and the spatial converged is also assured.

$$\begin{cases} \frac{\partial \mathbf{v}_\beta}{\partial t} + \mathbf{v}_\beta \cdot \nabla \mathbf{v}_\beta = -\frac{1}{\rho_\beta} \nabla p_\beta + \nu_\beta \nabla^2 \mathbf{v}_\beta \\ \nabla \cdot \mathbf{v}_\beta = 0 \\ \mathbf{v}_\beta = 0 \quad \text{on } x_1 = 0, L, x_3 = 0 \\ \mathbf{v}_\beta = U^{top} \quad \text{on } x_2 = L \\ \mathbf{v}_\beta|_{x_3=0} = \mathbf{v}_\beta|_{x_3=L} \\ p_\beta|_{x_3=0} = p_\beta|_{x_3=L} \end{cases} \quad (5.1)$$

OK

SPECIFICA
MEGLIO,
QUANTI
PUNTI DI
GRIGLIA
USI?
QUANTI TE
NE
BASTANO?

Once the system (5.1) is solved, the microscopic fields (velocity and pressure) inside the porous medium are averaged with the operator 5.2 in order to get the homogenized macroscopic field $\langle \mathbf{v}_\beta \rangle^\beta$ and $\langle p_\beta \rangle^\beta$.

$$\langle \psi_\beta \rangle^\beta = \frac{1}{V_\beta} \int_{V_\beta} \psi_\beta(\mathbf{x}) dV_\beta. \quad (5.2)$$

The operator (5.2) has been applied through the ~~all~~ porous domain using a REV with dimension $\ell \times \ell \times \ell$. It means that the centroid of the REV, in which the average operation is performed, spans all the porous domain extension. It should be noted that the averaging procedure gives a two dimensional averaged fields as results, the only non null values are in the x_1 and x_2 directions. This is due to the symmetry of velocity and pressure in the x_3 direction that return ~~null~~ zero averaged field as a result of the averaging operation (5.2).

5.2.2 Macroscopic approach though VANS

The same problem is solved using the VANS approach. The set of equation used are the incompressible Volume Averaged Navier-Stokes equations in the two dimensional case with

a Darcy-Forchheimer closure (5.3). The derivation of this set of equation has been already discussed in chapter 2.

$$\begin{cases} \frac{\partial \langle \mathbf{v}_\beta \rangle}{\partial t} + \frac{1}{\varepsilon} \nabla \cdot [\langle \mathbf{v}_\beta \rangle^\beta \langle \mathbf{v}_\beta \rangle^\beta] = -\frac{1}{\rho_\beta} \nabla \langle p_\beta \rangle^\beta + \nu_\beta \nabla^2 \langle \mathbf{v}_\beta \rangle^\beta \\ \quad -\nu_\beta \varepsilon \mathbf{H}^{-1} \langle \mathbf{v}_\beta \rangle^\beta + \frac{\nu_\beta}{\varepsilon} \nabla \varepsilon \cdot \nabla \langle \mathbf{v}_\beta \rangle^\beta + \frac{\nu_\beta}{\varepsilon} \langle \mathbf{v}_\beta \rangle^\beta \nabla^2 \varepsilon \\ \nabla \cdot (\varepsilon \langle \mathbf{v}_\beta \rangle^\beta) = 0 \\ \langle \mathbf{v}_\beta \rangle = 0 \quad \text{at } x_1 = 0, L, x_2 = 0 \\ \langle \mathbf{v}_\beta \rangle = U^{top} \quad \text{at } x_2 = L \end{cases} \quad (5.3)$$

The boundary conditions are the same as the DNS approach except for the x_3 dimension that in this case is neglected since the homogenized problem is already two dimensional. The solution of ~~the~~ system (5.3) gives directly the averaged velocity and pressure fields to be compared to the averaged DNS fields.

Interface treatment

The penalization method (or one domain approach) has been chosen to ~~treat~~ the interface of the porous medium. The method has been already discussed in section 2.5 of chapter 2 but here some technical aspect are further discussed. In order to use the so called penalization method the porosity field and the effective permeability ~~had~~ to be defined in all the domain. In the free fluid the porosity is, of course, unitary and the effective permeability infinite. With such a numerical values the Navier-Stokes system 5.1 is retrieved from the system 5.3 after some ~~simple~~ simplifications. In the deep porous medium the porosity is constant and set equal to 0.8. The effective permeability is also constant and the components of the tensor has been taken from a posteriori computation of the homogenized-DNS problem. This procedure involves the inversion of the Darcy system $\langle \mathbf{v}_\beta \rangle = \nu_\beta \varepsilon \mathbf{H}^{-1} \nabla \langle p_\beta \rangle^\beta$. The numeric values for \mathbf{H} are represented in table 5.1.

	$H_{11} = H_{22}$	H_{33}
$Re = 100$	$2.63 \cdot 10^{-2}$	$5.49 \cdot 10^{-2}$
$Re = 1000$	$2.65 \cdot 10^{-2}$	$5.63 \cdot 10^{-2}$

PERCHE' IN (5.5)
USI \mathbf{H}^* ??

Table 5.1: Apparent permeability values from table 1 in Zampogna and Bottaro [165]

The apparent permeability tensor \mathbf{H} is also diagonal. This is consistent with the result in chapter 4 in low pore Reynolds number, as a matter of fact in ~~all~~ the cavity ~~Reynolds numbers tested~~ the pore Reynolds number is always below 5, ~~for both cases tested~~. However it is difficult to define how to connect the different values for the free fluid and the porous media part through the interface. Although, the exact profile for the porosity ~~However~~

$$\left(\frac{d}{2\ell}\right)^2$$

filed can be computed known the geometry of the medium. In this case the porous medium is made of cylindrical fibers in a regular arrangement. The relationship between the porosity in the deep medium ε , the size of the REV ℓ and the cylinder diameter d is:

$$\left(\frac{d}{2\ell}\right)^2 = \frac{1-\varepsilon}{\pi}$$

OPPURE $\left(\frac{d}{\ell}\right)^2 = \frac{4}{\pi}(1-\varepsilon)$

With the above relationship is possible to define the porosity as a function of the vertical coordinate $x_2 = y$:

$$\varepsilon(y) = \begin{cases} 1 & y \geq (y_{itf} + \ell) \\ 1 - \frac{1-\varepsilon}{\ell} |y_{itf} - y + \ell| & (y_{itf} - \ell) < y < (y_{itf} + \ell) \\ \varepsilon & y \leq (y_{itf} - \ell) \end{cases} \quad (5.4)$$

DEFINISCI y_{itf} !

~~è~~ uguale a h ??

$$y_{itf} = h - \ell$$

??

for convenience.

The same expression has been used for the effective permeability field. Although in the equation (5.5) the inverse of the effective permeability has been used because doing so the value of this term in the free fluid is equal to zero (instead of infinity). As a matter of fact in the system (5.3) only the inverse of the effective permeability is needed.

The H_{ii}^* term in the equation (5.5) refers to the effective permeability components of the deep medium, reported in table 5.1.

$$H_{ii}^{-1}(y) = \begin{cases} 0 & y \geq (y_{itf} + \ell) \\ 1 - \frac{1}{\ell} |y_{itf} - y + \ell| & (y_{itf} - \ell) < y < (y_{itf} + \ell) \\ 1/H_{ii}^* & y \leq (y_{itf} - \ell) \end{cases} \quad (5.5)$$

The data analyzed in chapter 4 suggests that the components of \mathbf{H} are mostly driven by the porosity effect so it is fair to suppose that the same variability should be used for both the porosity and the permeability fields. This assumption justifies the choice of the same formulation for the interface treatment for the two different fields.

justifies

5.2.3 Cavity $Re = 100$ comparison

This section present the comparison between the microscopic and macroscopic ~~different approaches~~ approach for the cavity at $Re = 100$. Pictures 5.2 and 5.3 show the pressure gradient and the velocity fields for the two different approaches. Each field is made non-dimensional using the macroscopic length and the velocity on the top of the cavity:

$$u^* = u/U_{top}, \quad v^* = v/U_{top}$$

$$\frac{\partial p^*}{\partial x} = \frac{\partial p}{\partial x} / (0.5\rho_\beta U_{top}^2/L), \quad \frac{\partial p^*}{\partial y} = \frac{\partial p}{\partial y} / (0.5\rho_\beta U_{top}^2/L)$$

119

Secondo me

$$h = y_{itf}$$

$$\varepsilon = 0.8$$

$$\varepsilon = 1$$

$$\varepsilon(y) = \frac{0.2}{\ell} (y - y_{itf}) + 0.9$$

e simile per H_{ii}^{-1} ...

valide per

$$y_{itf} - \frac{\ell}{2} \leq y \leq y_{itf} + \frac{\ell}{2}$$

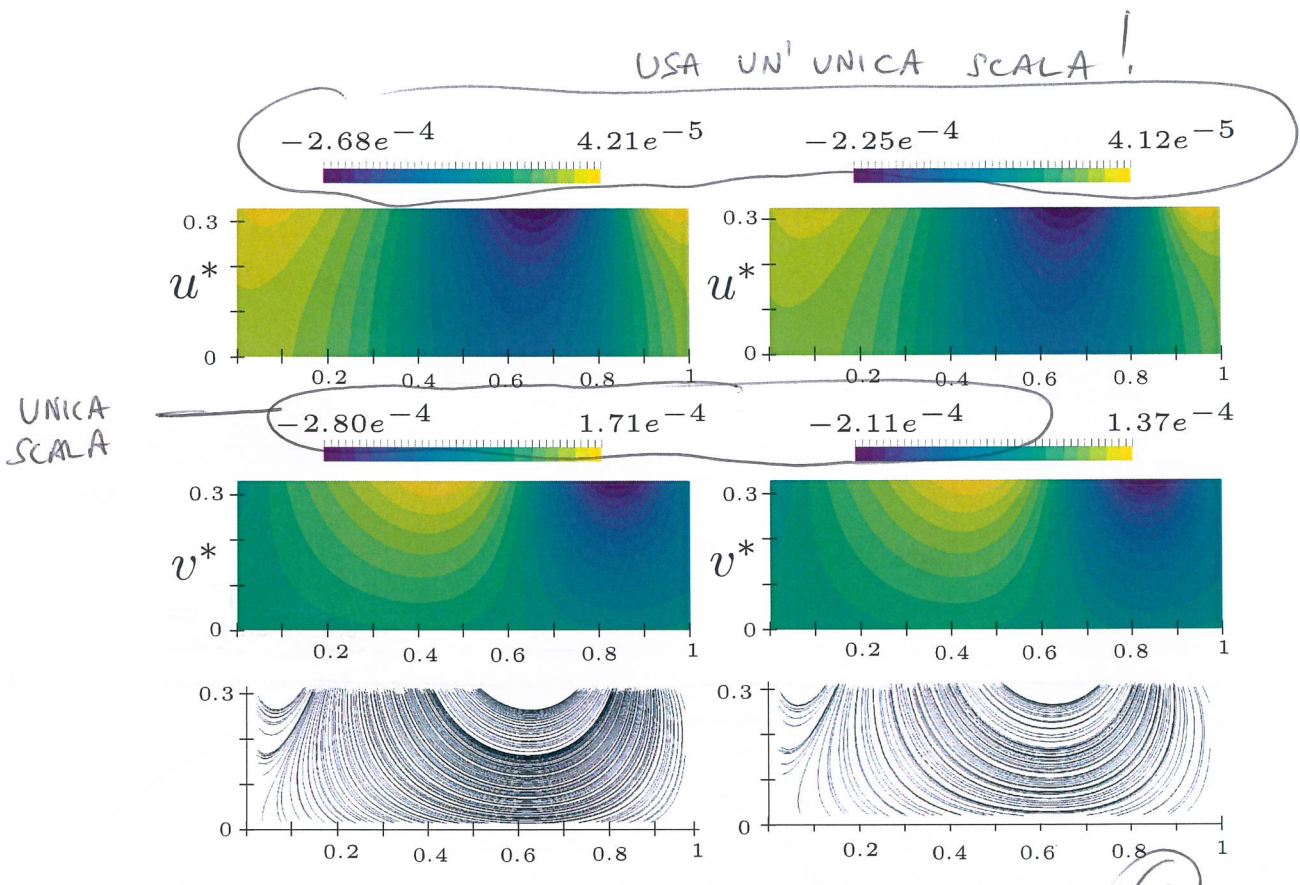


Figure 5.2: Left: VANS approach. Right: Homogenized DNS approach. The figure shows, from top to bottom, the horizontal velocity the vertical velocity and the streamlines inside the porous domain Ω_p

The DNS approach is used as reference case for the comparison. At Reynolds number equal to 100 we have a ~~fair~~ agreement in the velocities and pressure gradients fields. The contours and the location of the local minima and maxima are the same for the two approaches. If we look at the numerical values, for some fields the relative errors are not negligible; however, they are, in mean, always below 10%. Also the flow path inside the porous domain is in good agreement with the DNS data. Some differences between the two models has to be expected since in the VANS approach the micro-scale flow behavior is modeled. This means that some of the details that the full DNS is able to retain, are lost in the macroscopic approach.

have

FATI VEDERE ANCHE
COSA SUCCIDE NEL FLUIDO
(DOVE $\epsilon = 1$) E FATI VEDERE
120 ALCUNE IMMAGINI CON
PARAGONI ATTORNIO
ALL'INTERFACCIA ...

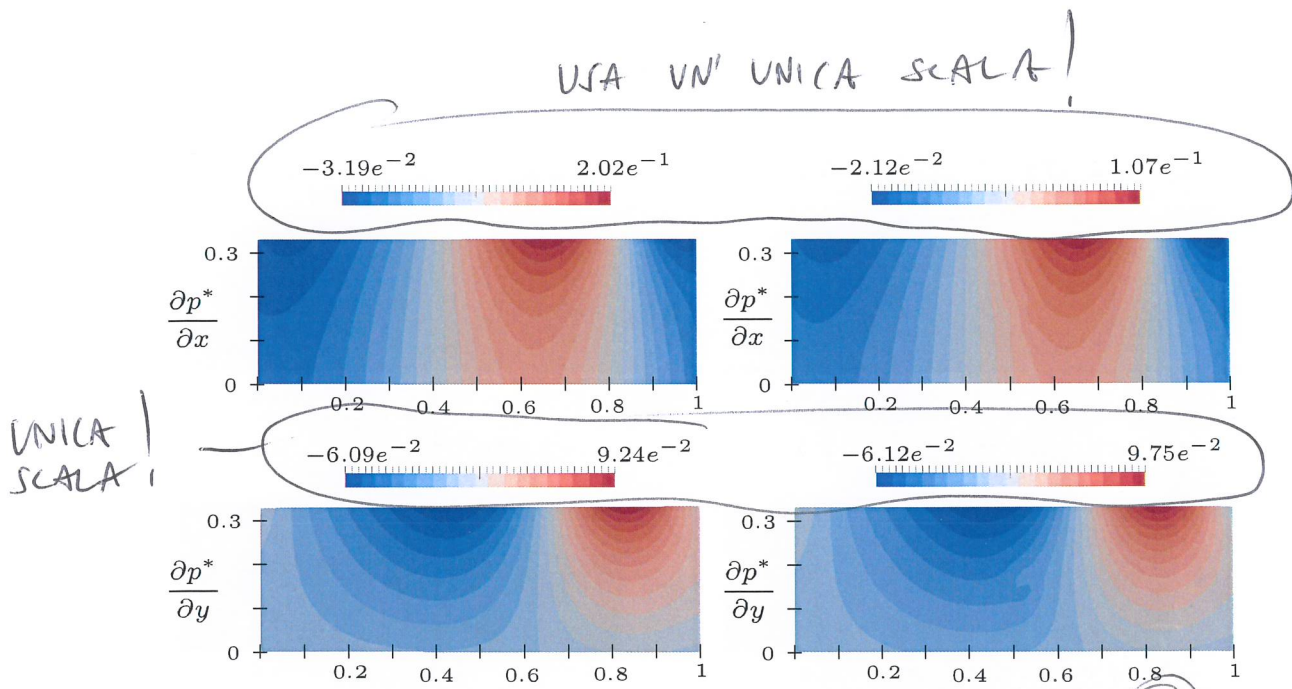


Figure 5.3: Left: VANS approach. Right: Homogenized DNS approach. The figure show, from top to bottom, the horizontal and the vertical component of the pressure gradient inside the porous domain Ω_p

5.2.4 Cavity $Re = 1000$ comparison

The same case and comparison has been done also for a Reynolds number equal to $Re = 1000$. For this case the same conclusion as the previous case are confirmed. Some of the relative errors are even smaller compared to the previous Reynolds number case. This support the robustness of our model in this range of Reynolds number. These two solutions of the cavity problem shown that varying the permeability in a linear manner through the interface is ~~the better~~ choice when using the penalization method.

an acceptable

and the porosity

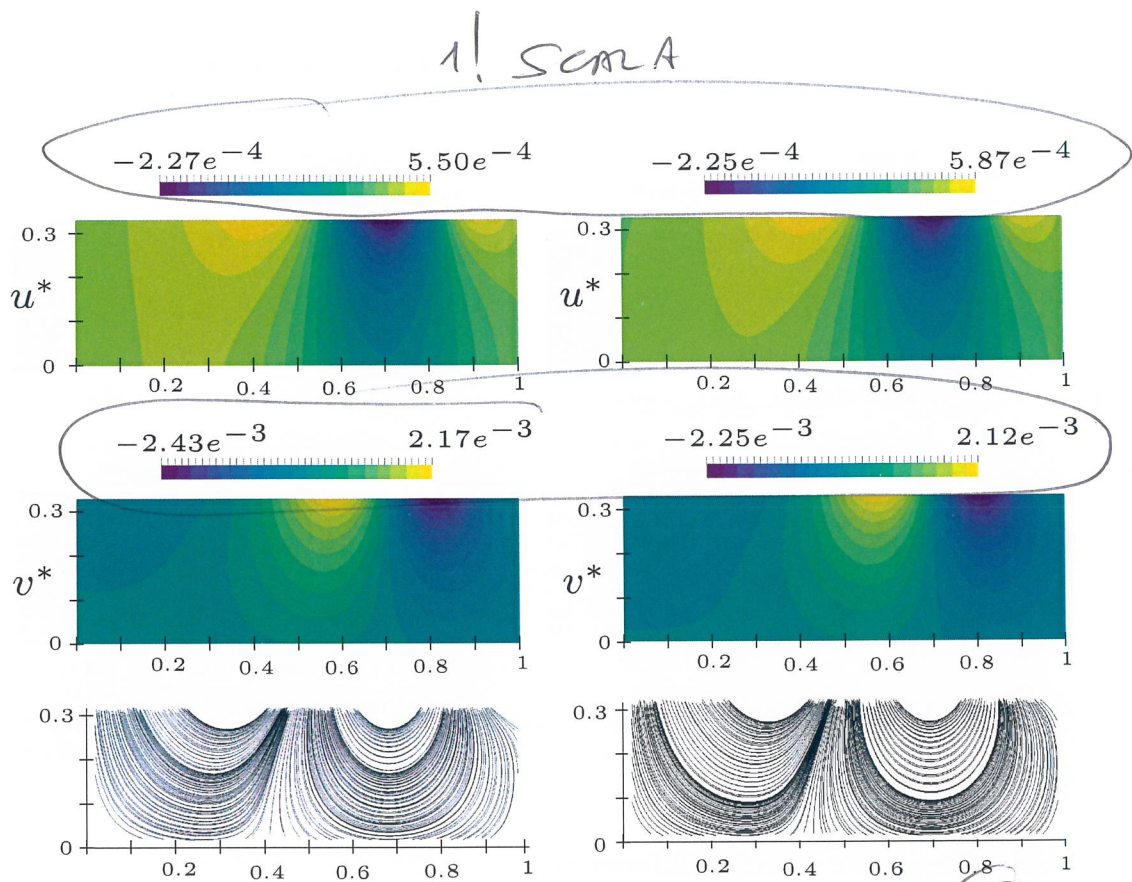


Figure 5.4: Left: VANS approach. Right: Homogenized DNS approach. The figure show, from top to bottom, the horizontal velocity the vertical velocity and the streamlines inside the porous domain Ω_p

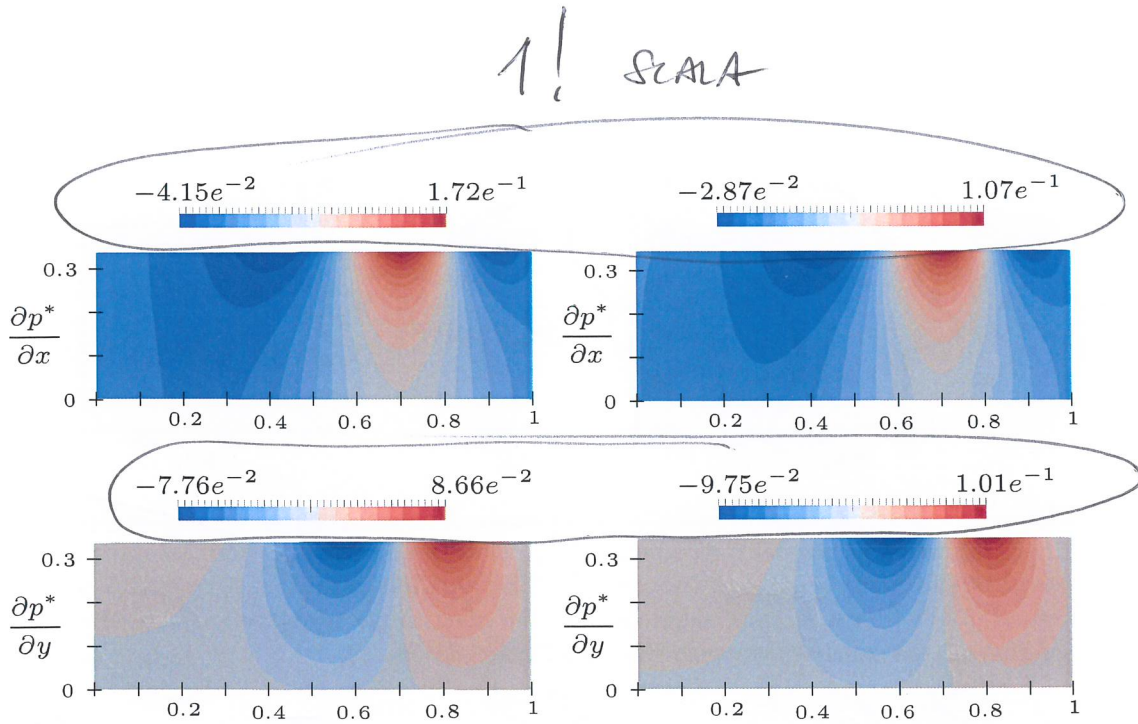


Figure 5.5: Left: VANS approach. Right: Homogenized DNS approach. The figure show, from top to bottom, the horizontal and the vertical component of the pressure gradient inside the porous domain Ω_p

5.2.5 Cavity $Re = 5000$ using H metamodel

In our previous simulations the metamodel for the effective permeability has not been applied. As a matter of fact the metamodel in chapter 4 was built for a porous medium made of staggered cylinders. So it would not be applicable when the porous medium is made by regular arranged cylinders.

In order to test how the effective permeability would impact our model we show the solution for another test case. In the same cavity geometry as before the system (5.3) is solved with or without the Kriging metamodel for the effective permeability.

Although we have seen that at low pore Reynolds number the effective permeability is practically not sensitive to variation of flow direction and/or magnitude¹. For this reason also the Reynolds number has been increased to 5000, that is still in the stationary regime but is near the transition limit (Yih-Ferng et al. [163]).

Figure shows the velocity and permeability profiles for a sample cut made at the center of the cavity at $x = 0.5L$. It is clear that the macroscopic velocity is not affected by the different treatment of the permeability, as a matter of fact the two velocities can be superposed almost precisely. Although the inverse of the effective permeability component show some differences. At the interface it is possible to see also how the trend of the two

¹see figures 4.10, 4.10 and 4.10 in chapter 4

However,
123
Kriging
MINUSCONE

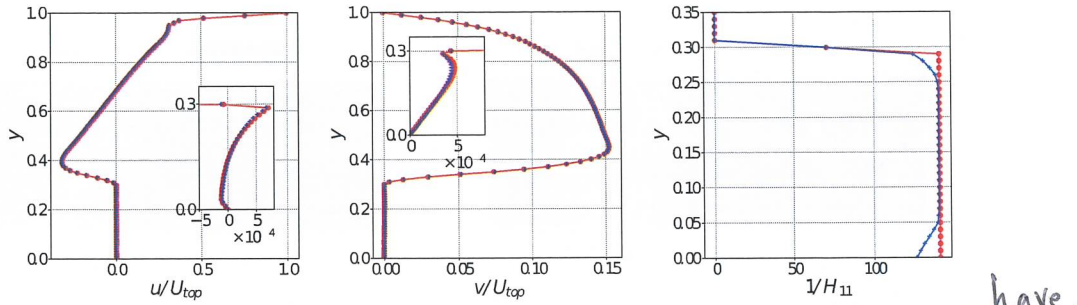


Figure 5.6: Left: horizontal velocity component. Center: vertical velocity component. Right: Effective permeability component $1/H_{11}$. The three fields have been sampled at the center of the cavity geometry, $x_1 = 0.5L$. The blue line represents the solution for the system (5.3) with the Kriging metamodel for the effective permeability, the red line is the solution to the same system with the model switched off.

different treatment look like ~~the same~~ at the interface. Although the permeability start to increase at a deeper vertical position than the case without metamodel. This is caused by the vertical angle ϕ that is near to 90° at that point because of the fluid penetration. The analysis made in chapter 4 shows that the permeability increase when the angle ϕ increases. However the value of the permeability deep in the medium is almost the same. In any case even if there are some differences in the permeability profiles this seems not to affect the averaged velocities.

The fact that with the Kriging metamodel the same linear profile as equation 5.5 is retrieved is another confirmation that the linear variation is ~~the right choice~~ acceptable.

5.3 Separated flow between hills

In chapter 1 we have presented some flow examples where a porous media layer in the leeward side of a bluff body can reduce the separation extension. In order to test the effectiveness of our model to make predictions in this sense, the flow over periodically arranged hills has been chosen as test problem. This configuration has been already investigated experimentally and numerically and is a classical CFD ~~benchmark~~ problem now standardized by the ERCOFTAC committee. It is used as a benchmark case to investigate the ability of DNS, RANS and LES models to resolve separation from a curved geometry. The flow field features a large separation bubble caused by the curved surface of the hill and a natural reattachment in the flat part between the two hills crests. The flow is assumed to be periodic and two dimensional, at the Reynolds number tested. Numerous DNS and LES works can be found in literature with Reynolds numbers up to 10000 (Chang et al. [39], Breuer et al. [24], Breuer et al. [25] and [14]). This test case has been studied with two

$$[4, 25, 16^2] \text{ and } [124]$$

main objectives to test the modeling and simulation issue related to our VANS solver and the physical capacity to reproduce the flow field behavior. Our idea is to extend the hill profile with a porous media layer and assess how the separation bubble is modified by the layer presence. ~~influence~~ We have tested small Reynolds number in the laminar regime. Although the problem has been chosen especially for the possibility to future extend the study to higher Reynolds numbers since a lot of data can be found in literature to validate the result.

Geometry and conditions

The geometry of the problem is depicted in figure 5.7. It is two dimensional since the Reynolds number considered is in the laminar regime and the flow does not present any three dimensional characteristic in this range. The dimension of the hill crest and extensions are also showed in the same pictures being non-dimensional with the hill crest height. The chosen dimensions of our setup are: $L_x = 9.0$, $L_y = 3.036$ and $h = 1$ where x, y, z are the streamwise, wall-normal and spanwise direction, respectively. We solve the flow inside of a single streamwise periodic segment and thus covers solely one complete hill region from crest to crest. Between one hill and the next one there is a flat plate region of extension $5h$. The pressure-induced separation takes place from the first hill curved surface and reattachment is observed at the flat plate part between the two hills.

The hills profile is described by a polynomial parametric curve function of the streamwise direction $y_{hill} = f(x)$. The specific coefficients and definition can be found in Almeida et al. [4]. This geometry is also named **base** case in the following text.

The problem is discretized using the finite volume method implemented in OpenFoam and the mesh used is shown in figure 5.7. The mesh is purely made of hexahedral cells and counts 25000 elements in the two dimensional version. It is possible to download it at https://turbmodels.larc.nasa.gov/Other_LES_Data/2dhill_periodic.html. The resolution has been already validated in DNS and LES computations so it has not been further investigated here.

The inlet and the outlet patches are connected with a periodic boundary condition, at the hill and flat plate surface the no-slip condition is imposed and finally at the top of the domain a slip condition is used. The numerical setup for the numerical scheme and linear solvers is the same as the DNS simulations in chapter 4, paragraph 4.3.2.

The equations solved are a slightly modified version of the VANS system (5.3) in which the constant macroscopic pressure gradient is introduced as a source term in the momentum. The non-periodic behavior of the pressure field can be accounted for by adding the mean pressure gradient as a source term to the momentum equation in streamwise direction.

equation.

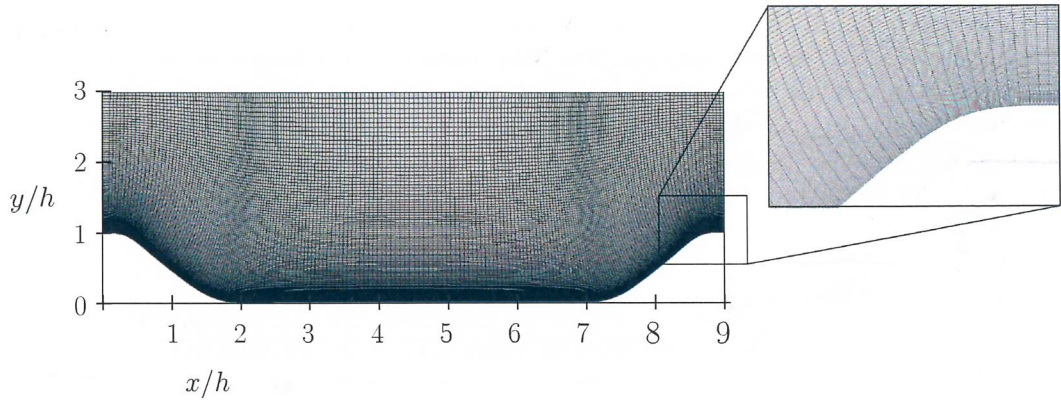


Figure 5.7: Domain of the problem and mesh used to discretize it. On the right side there is an enlargement of the zone on the hill curvature.

$$\begin{cases} \frac{\partial \langle \mathbf{v}_\beta \rangle}{\partial t} + \frac{1}{\varepsilon} \nabla \cdot [\langle \mathbf{v}_\beta \rangle^\beta \langle \mathbf{v}_\beta \rangle^\beta] = -\frac{1}{\rho_\beta} \nabla \langle p_\beta \rangle^\beta + \nu_\beta \nabla^2 \langle \mathbf{v}_\beta \rangle^\beta \\ \quad -\nu_\beta \varepsilon \mathbf{H}^{-1} \langle \mathbf{v}_\beta \rangle^\beta + \frac{\nu_\beta}{\varepsilon} \nabla \varepsilon \cdot \nabla \langle \mathbf{v}_\beta \rangle^\beta + \frac{\nu_\beta}{\varepsilon} \langle \mathbf{v}_\beta \rangle^\beta \nabla^2 \varepsilon - \mathbf{g} \\ \nabla \cdot (\varepsilon \langle \mathbf{v}_\beta \rangle^\beta) = 0 \\ \langle \mathbf{v}_\beta \rangle = 0 \quad \text{at hill wall} \\ \frac{\partial u}{\partial y} = 0 \quad \text{at } y = 3.035h \quad \text{SPAZIO} \quad 3.036 ? \\ \langle \mathbf{v}_\beta \rangle|_{x_1=0} = \langle \mathbf{v}_\beta \rangle|_{x_1=9h} \\ \langle \mathbf{v}_\beta \rangle|_{x_1=0} = \langle \mathbf{v}_\beta \rangle|_{x_1=9h} \end{cases} \quad (5.6)$$

In the system (5.6) the flow is driven by the source term \mathbf{g} and the Reynolds number is computed a posteriori in the following manner:

$$R_e = \frac{U_b h}{\nu}$$

where U_b is the velocity in the top left corner of the domain, just above the first hill.

The treatment for the porosity is the same as equation (5.4) where in this case the y_{itf} is described by two different profiles. The first one, ~~the hill~~, called **external**, is the same hill profile translated to the right by a length equal to $0.2h$ in the streamwise direction. This setup is used to test the case of a porous media layer on the external part of the hill. In this case the hill geometry is modified.

In the second case the interface profile y_{itf} is exactly the hill profile at the same position and the ~~the~~ solid part of the hill is translated in the direction $-x$ by $0.2h$. In this setup,

denoted internal,
BOLD

the porous media layer has been inserted on the "inside" of the hill leeward side. It means that the total geometrical extension of the hill plus the porous media layer is the same as the base case described by y_{hill} .

The porous media layer has the same geometry of the one described in 4, a series of cylinders in staggered arrangement. The cylinders are then arranged on the leeward side of the hill and they are aligned with the wall normal direction. Although their extension is not uniform, the line that passes through all the cylinders lid describe the curves y_{itf} external and internal.

The two different porosity field arrangements are depicted in figure 5.8. Where the porosity deep inside the medium, showed in green, is equal to 0.8 and the exterior porosity field is equal to 1 and is showed purple.

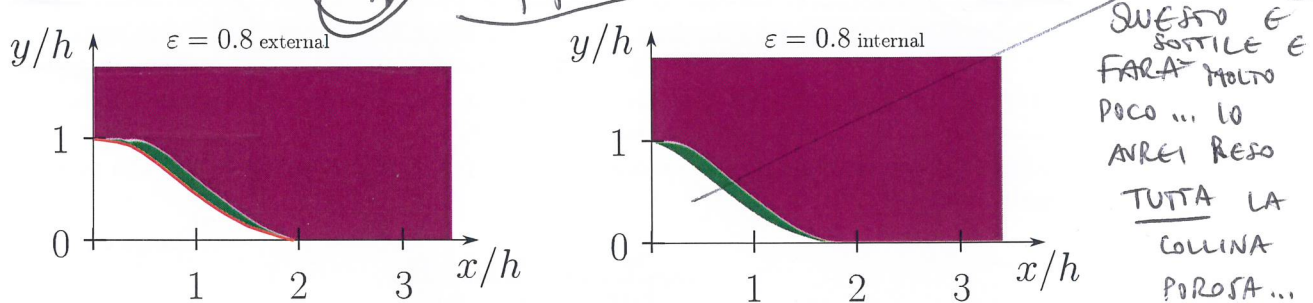


Figure 5.8: Porosity field in the leeward side of the first hill for the two different cases *external* and *internal*. The porosity in the deep medium is equal to 0.8 and is colored in green, instead the porosity in the free fluid is equal to 1 and it is colored in purple. On the left case, the *external* one, the red line describes the hill profile of the base case and the white line describes the porous media interface. For the *internal* case on the right the base hill profile and the porous media interface are the same one, and they are depicted in white.

On figure 5.8 the left picture shows the case named *external*, the red line indicate the hill profile in the base case and the porous media layer is put on top of it and the white line indicate the porous media interface y_{itf} . The right picture in figure 5.8 instead shows the configuration in the case named *internal*. For this case the porous media interface line y_{itf} is the same as the hill profile in the base case and is depicted in white.

To summarize the two different cases differ for the position on the porous media interface that is equal to the hill profile translated in the positive streamwise direction (case *external*) or in the negative streamwise direction (case *internal*). The translation has the same extension of $0.2h$ for each case.

The interface has also been treated with the linear smoothing function (5.4).

The permeability tensor components are then evaluated with the Kriging metamodel in the zone where the porosity field is different from one. ~~that describe indeed the porous~~

Summarize

CE LA FAI A
FARE UN ALTRO CASO
CON TUTTA LA COLLINA

(A MONTE E A VALLE) POROSA?

debbie

its

5.3.1 Comparison between smooth and porous leeward side of the hill

The above geometrical setup has been studied in the stable laminar regime. In this case the source term is equal to $\mathbf{g} = (0.5 \cdot 10^{-9}, 0, 0)$ that results in a Reynolds number equal to 83. For all the cases the recirculation bubble has been measured in ~~his~~ vertical and horizontal extension. The horizontal extension L_R is defined as the first streamwise point in which a sampled velocity profile shows only positive streamwise velocities. The vertical extension has been measured at $x = 4.5$ that is the mean extension of the domain. Table 5.2 collects these results. Looking at the results the porous media has a negative effect in both either in L_R and $h_{x=4.5}$. For the case *external* the geometry of the hill is modified indeed by the porous medium and the leeward side is pushed downstream so it is not surprising that the recirculation extension is pushed downstream ~~itself~~. Although the same negative effects can be found also for the *internal*. This is line with some observation made by Jimenez et al. [85] and Gomez-de Segura et al. [70] in which they ~~argue~~ that some configuration of the porous surfaces characteristic (porosity and permeability) can produce negative effects.

A similar negative

argues

case	L_R	$h_{x=4.5}$
base	5.6	0.27
external	5.95	0.33
internal	5.8	0.31

Table 5.2: Recirculation bubble streamwise extension L_R and vertical extension at $x = 4.5$ for the three porous media configurations.

within

The streamlines in figure 5.9 show the shape of the recirculation bubble for the three cases. It can be seen that they look very similar and as a matter of fact the differences described in table 5.2 are ~~around the 5% difference~~ from the base case without the porous layer. In figure 5.10 the local velocity fields are analyzed. The sampled velocities at $x = 1$ seems very different because the geometry in that point is not the same. Although ~~I~~ we look at the horizontal velocity gradients ~~are~~ similar. Some differences can be shown for the vertical velocities. The *internal* case presents smaller vertical velocities than the other two cases at $x = 1$, ~~is~~ close to the detachment point. The situation is inverted further downstream at $x = 2$ and the three profiles collapse ~~one~~ into another at $x = 3$. This different local behaviors can be used for example in situations where the vertical exchange of momentum has to be enhanced for examples in aquatics plant applications where the nutrient exchange has to be optimized.

observed

onto one another

STRANGE

APPLICATION ...

, they are

*E se tutto lo colline
fosse proso?*

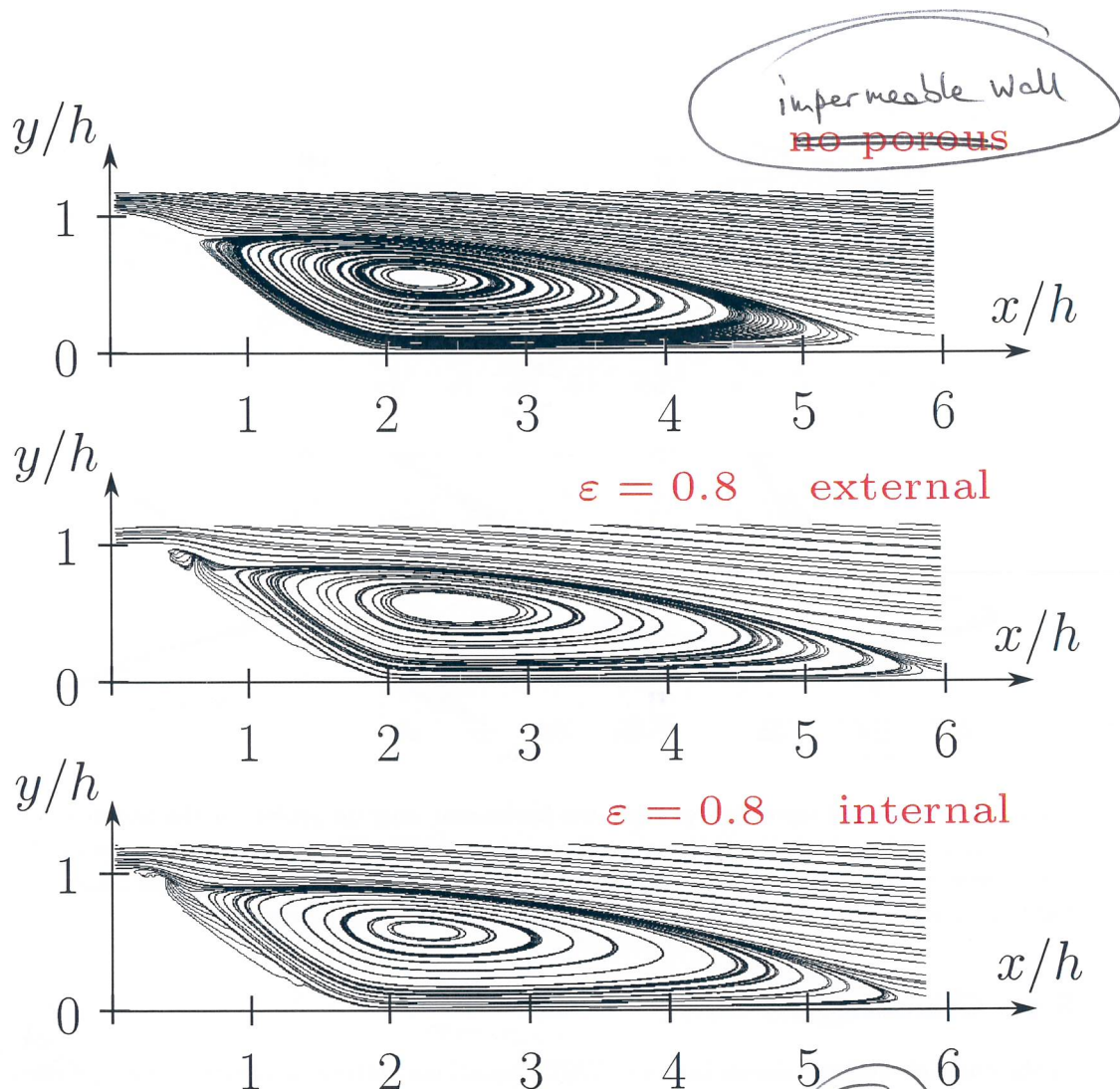


Figure 5.9: Streamlines for the three cases tested. The top picture shows the case without the porous medium. The central picture shows the case where the porous media layer is put on the external part of the leeward side and the bottom case shows the case with porous medium put inside the leeward side.

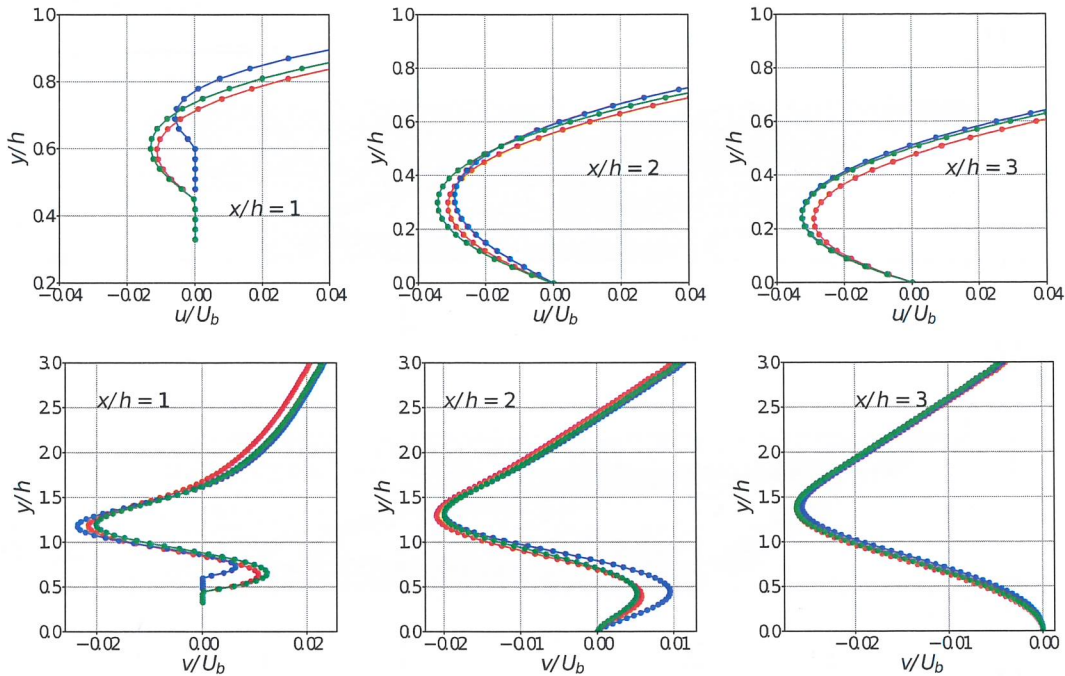


Figure 5.10: The top three figures show the horizontal velocity profile for the sampled cut at $x = 1$, $x = 2$ and $x = 3$ respectively from left to right. The bottom figures follow the same patterns but instead shows the vertical velocity profile. The red line is the **base** case the blue line is the **external** case and the green line is the **internal** case.

5.4 Conclusions

In the chapter we have shown how the VANS equations derived in chapter 2 can be used to describe the averaged macroscopic field for rigid porous medium. We have also shown how the interface should be treated in order to retrieve good results. Direct comparison with DNS data show that the linear smoothing of ~~other~~ the porosity filed and the effective permeability filed are necessary. We have also shown that using the metamodel developed for \mathbf{H} produce the same smoothing for the interface. Finally the periodic hill application ~~show~~ demonstrate that our homogenized solver can be used easily as a tool to test and measure porous coating and their effectiveness. For the porous characteristic used in our test we have found that the porous medium has negative effects for separation. But our focus were posed on the validation ~~of the correctness~~ and easiness-to-use of our macroscopic model. With this tool, is now possible to extensively study this porous media coating in order to find the optimal characteristics for different objectives.

Chapter 6

Conclusions, recommendation and discussions

6.1 Main conclusions

In chapter 1 we have reviewed the latest advances and open questions present in literature. The same chapter forms a new and improved basis from which many researchers could find and/or explore new research paths and ideas. In this final chapter we list the main results and conclusions that have been drawn from our work.

- The volume averaged method has been detailed in key hypothesis. The mathematical procedure needed to find the macroscopic equations, and the closure problem, has also been presented. Some of the most notable new extensions to the method have been included in the discussion that we hope it could help new researchers to approach the study of this method and serve as a review for who is already accustomed to it.
- The sensitivity analysis shows that the VANS approach is the less sensitive one with respect to variations in the base flow. Also, the stability results agree with the experimental results. One of the possible drawbacks in the use of the VANS model is the need of computing the effective permeability tensor \mathbf{H} , although even the parametrization of the drag force is not an easy task. The computational cost and difficulties to compute the components of the permeability tensor is the main reason that have taken us in the development of a metamodel for the tensor \mathbf{H} in chapter 4.
- Opposed to the results in the work of Lasseux et al. [96] for rectangular fibers, our computed effective permeability tensor for circular fibers is diagonal. This means that the geometrical shape of the porous structure is very important in this sense. A possible generalization of different porous structures is shown in Pauthenet et al. [125] even though further investigations on the non diagonal terms are needed.

toward

128

to a good approximation

- We have also shown that the 3D effects can be very important in changing the permeability tensor components. In our data analysis, in chapter 4, we have shown that the angle ϕ ¹ has a big influence in the tensor \mathbf{H} components, especially in the inertia regime. The same angle ϕ , when present, makes the flow three dimensional and it bends the fluid path along the fiber axis. This process translates into a non-zero deviation angle γ in the fiber axis direction.

• In chapter 4 we have shown that the \mathbf{H} metamodel has been developed up to a Reynolds number equal to 100. This limit has been derived from the data and it was not fixed a priori. To estimate this limit we have checked the direct comparison of F^m and F^M since it is a fair estimation of the correctness of the hypothesis behind our closure model. For our geometry and range of porosities tested, the correct limit is around Reynolds number 100. After this limit the error between the two quantities starts to be appreciable and so the closure problem (2.49) is no more correct. We suppose that at higher Reynolds number the linear correlation hypothesis between the averaged and perturbation (equations (2.39) and (2.40)) does not hold.

- The interface treatment, based on the penalization method, has been investigated in chapter 5. It has been shown that the double linear smoothing of ~~the~~ porosity and ~~the~~ permeability has a positive effect on the correctness of the homogenized model. We have also shown that the linear porosity profile derive directly from the geometry of the porous media and it is exact. On the contrary the linear smoothing for the permeability tensor is purely heuristic, but it can be supported by the fact that the porosity effects are largely the most important in the variability of \mathbf{H} . So it is possible to argue that the two fields should have the same interface treatment. Another confirmation for this fact comes from the metamodel that if left "free" it return the linear profile at the interface without previously imposing it *a priori*.

- REALLY?
- The inclusion of a porous media layer has been tested and the solver had shown good computational performance and no convergence problems has been found. However, the physics of the separation is not much modified by the porous layer. This finding suggest that the laminar suppression mechanism could be not as effective as the turbulent one (already observed in literature). In any case, more simulations with different parameters and different problem geometries are needed to generalize the results.
- Our VANS approach has been tested in geometries that naturally develop separation. The inclusion of a porous media layer has been tested and the solver had shown good computational performance and no convergence problems has been found. However, the physics of the separation is not much modified by the porous layer. This finding suggest that the laminar suppression mechanism could be not as effective as the turbulent one (already observed in literature). In any case, more simulations with different parameters and different problem geometries are needed to generalize the results.
 - The OpenFoam implementation of the macroscopic solver based on the VANS equations can be downloaded from github from the address: https://github.com/appanacca/porous_solvers_OF. The code listing is not directly shown in the manuscript since detailing the solver implementation would require to explain lot of OpenFoam library technicalities. These details has been already addressed in multiple sources

¹the angle between the forcing term in the momentum equations and the fiber axis

[101, 115]

(Jasak [84], Moukalled et al. [115] and [101]) and they are out of the scope of this work. ~~Although~~, To someone not new to OpenFoam programming the comments inside the code listing are sufficient to clarify the technical points.

6.1.1 Possible future research extensions

- The database from which we have built our metamodel for the tensor \mathbf{H} can be extended. For example we could easily include more data points to make the model more reliable. Another interesting part could be the extension to other fibers geometry section or even other completely different porous media geometries (spheres, rocks ...). The database could also be extended to moving porous media, the input parameters could include some of the typical dynamic parameters like the mass ratio and the stiffness of the fibers. New metamodeling approaches could also be explored, especially as the database ~~now~~ deep neural networks could perform better than Kriging.
- The validation of the interface treatment need more data from DNS simulations or experiment in similar configurations. The availability of high resolution data is still a missing piece in the field.
- The application of the macroscopic model to separated flow is only a starting point. We have shown that our model is capable of providing fairly correct homogenized flow field at a low computational cost. Although the capacity of a porous media layer to suppress the separation is still questioned, at least with the parameters used. This means that the optimal parameters are still to be found. An optimization procedure using the adjoint equation could solve this problem, now that we have clarified the penalization approach used in the VANS equations.
- Another possible extension to the metamodel could be the implementation of the algorithm 1 for elastic porous media. Since the VANS solver is already been implemented this extension using a Bernoulli beam should be fairly easy.

